IEEE Access
Multidisciplinary ⋮ Rapid Review ⋮ Open Access Journal

Received April 3, 2022, accepted April 13, 2022, date of publication April 21, 2022, date of current version April 28, 2022.

Digital Object Identifier 10.1109/ACCESS.2022.3169161

Gearshift Control in Engagement Process of Dual-Motor Coaxial Propulsion System for Electric Bus

CHENG LIN, JIANG YI, XIAO YU, AND HUIMIN LIU
National Engineering Laboratory for Electric Vehicles, Beijing Institute of Technology, Beijing 100081, China
Collaborative Innovation Center of Electric Vehicles in Beijing, Beijing Institute of Technology, Beijing 100081, China

Corresponding author: Xiao Yu (rmyuxiao@163.com)

This work was supported in part by the National Natural Science Foundation of China under Grant 51975049.

ABSTRACT Considering single-motor drive system cannot meet the requirements of high-performance electric buses for Beijing Winter Olympics, a dual-motor coaxial propulsion system based on single planet gear set is developed. At the same time, a shift control method based on hierarchical linear quadratic regulator (HLQR) algorithm is designed to improve the poor shift quality caused by the rapid change of output shaft speed in the shift process. In this method, the upper controller adopts robust tracking linear quadratic regulator algorithm to control the speed change rate of the output shaft in the process of gear shifting, so as to reduce the load of gear shifting actuator in the process of gear shifting; the lower controller adopts disturbance suppression linear quadratic regulator algorithm to control the shifting force and improve the adaptability of the system to disturbance conditions Through simulation analysis, the performances of hierarchical linear quadratic regulator algorithm, optimal control algorithm based on variational method and PI algorithm in the process of gear shifting were comparatively analyzed. Simulation results showed that the hierarchical linear quadratic regulator algorithm exhibited a better performance in gear control than the other two algorithms. In addition, a large number of bench test results also proved that compared with PI algorithm, hierarchical linear quadratic regulator algorithm reduced vehicle impact by 19.17% and reduced the shift force by 32.48% in the sacrifice of shift time by 5.03%.

INDEX TERMS Beijing Winter Olympics, dual-motor coaxial propulsion system, hierarchical linear quadratic regulator algorithm, process of gear shifting, single planet gear set.

I. INTRODUCTION

Electric vehicles (EVs) are widely considered an effective approach to solve the problem of environmental degradation and energy shortage [1]. Related policy has been issued to encourage the development of electric vehicle industry in many country [2]. Currently, the popularization of electric vehicles is mainly limited by the endurance mileage and battery safety. With the increase in market demand, it is urgent to promote the system efficiency and power density of EVs. Considering the architectures of EVs in application, the centralized driving form of power unit is widely used at first since it inherits plenty of features from traditional vehicles [3]. In order to meet the requirements of climbing ability and cover the all-speed range of power system, the integration of motor and conventional transmission is conducted, which has excellent potential and superiorities [4], [5].

Recently, dual-motor transmission system has become more popular trend than single motor integrated system because of better energy-saving and dynamic performance [6], [7]. The dual-motor integrated system can achieve uninterrupted gear-shifting process and reduce energy consumption by accurate power allocation strategy [8]. Xu *et al.* proposed a novel electric dual-motor transmission system consisting of 5 single motor modes and 4 dual motor modes for heavy commercial vehicles [9]. Wu *et al.* proposed two novel dual-motor input powertrains based on dual-motor with planetary gear transmission (DMPGT) and parallel axel transmission (DMPAT), respectively, and found that the EVs with proposed dual-motor input powertrains had higher overall

The associate editor coordinating the review of this manuscript and approving it for publication was Yangmin Li.

efficiency than the EVs equipped with single motor input powertrain [1]. Hu *et al.* designed a dual-motor four-speed transmission integration system concurrently driven by two motor for fully electric vehicles and hybrid electric vehicles, which has better performance in terms of energy consumption and vehicle acceleration compared with single-speed system [10]. In Ref. [11], [12], a dual-motor powertrain coupled with a planetary gear or a shaft-fixed gear unit is presented. Its mode switching relies on the exact action of two clutches and a synchronizer sleeve. The above studies have clarified that dual-motor-transmission systems are beneficial for achieving uninterrupted gear-shifting process and have great potential in improving energy efficiency. However, the above researches mainly focus on configuration design and gearshift rule extraction, without consideration on specific gearshift control strategy.

In the research of gearshift control strategy, the optimization of power interruption time, vehicle jerk, and other indicators to improve gearshift quality is the key. Hong *et al*. applied the time-optimal hybrid minimum principle in the controller [13]. In Ref. [14]–[16], an optimal gearshift control strategy designed which includes a PID controller or robust two degree-of-freedom (dof) controller based on the dynamics model and gearshift objectives. Then Mishra *et al*. presented a model-based automated calibration algorithm and applied it as core Iterative Learning Control (ILC) for gearshift process [17]. Zhao *et al*. proposed a gearshift control architecture combined with multi-objective trajectory planning by taking gearshift duration jerk and friction work as optimization objectives [18]. Nguyen *et al*. developed a coordinated control strategy to handle the requirements of optimal shift schedules and corresponding mode selection maps [19]. The simulation results showed the coordinated control strategy eliminated all torque gaps in the gearshift process. Li *et al*. proposed a coordinated driving motor speed and gearshift motor displacement control strategy for the integrated motor-transmission (IMT) system during the gearshift process [20]. Tian *et al*. investigated the optimal coordinated gearshift control of a seamless two-speed motor-transmission system for EVs. The strategy is developed based on optimal controllers, which is normally used to achieve high-quality gearshift process in the torque phase and inertia phase, respectively [21]. Choi *et al*. proposed a method for estimating transmission torque, which can adaptively compensate for the changing factors in gearshift process [22]. Wu and Zhang. built a rigid dynamic model of planetary-dual motor powertrain to formulate a general energy management strategy (EMS) and a robust EMS that can avoid the drastically change of motors speed, and proposed a speed feedback control strategy to improve gearshift quality [23]. Roozegar and Angeles. developed a gearshift control scheme for a novel multi-speed transmission system (MST) of EVs, and the main advantages of MST are simplicity and modularity [24]. Li *et al*. designed an active disturbance rejection control method for the complex motor-transmission system and uncertain gearshift process [25]. In Refs [26], a cooperative control strategy for the gear shift is proposed and a robust multivariable controller is designed as the upper-level control to treat the coupling effects effectively, in spite of the presence of model uncertainties and disturbances. Lin *et al*. propose a modified trajectory tracking control method with current feed forward active disturbance rejection control (CFF-ADRC) to carry out the optimized shift force trajectories to achieve optimized gearshift [27].

In summary, the following research gaps are identified based on the literature review:

1) The above researches ignore the influence of the output shaft speed state on the gearshift process. According to the experimental data, this study finds the problem that the speed transformation rate of output shaft will cause the reduction of shift quality or even the failure of shift;
2) The control methods in literature review are optimal control methods aiming at improving shift performance without considering shift reliability;
3) The optimal shift control model considering external disturbance is generally a coupled model, which needs to be decoupled.

The main research of this paper includes the following aspects:

1) A special electric drive system architecture is designed for the special application scenarios of 2022 Beijing Winter Olympics;
2) Aiming at the time-varying characteristics of the load in the gearshift process, a control strategy based on the hierarchical LQR controller is proposed;
3) The upper layer of the controller robust tracking linear quadratic regulator (RTLQR) algorithm to control speed change rate of output shaft in the gearshift process, thus reducing the load in engagement process. The lower controller adopts disturbance suppression linear quadratic regulator (DSLQR) algorithm to control shifting force and improve the system adaptability to the disturbance conditions;
4) The influence of different control methods on the gearshift process is analyzed, and the accuracy of proposed hierarchy LQR controller is verified by the test results.

II. POWERTRAIN CONFIGURATION AND DYNAMICS MODEL

Based on the dual-motor-transmission system and multi-dimensional optimization theory, this paper proposed a Dual-Motor Coaxial Propulsion (DMCP) system, which can provide multiple modes to deal with complex operating conditions to meet the special application scenarios of 2022 Beijing Winter Olympics. In addition, the biggest advantage is that the system can achieve gearshift without interruption. The DMCP application scenario as shown in Fig.1.

A. CONFIGURATION AND OPERATING PRINCIPLES OF DMCP

The configuration of the DMCP is shown in Fig.2, which mainly consists of an Auxiliary Motor (AM) and a Traction Motor (TM). In addition, a two-gear planetary transmission is connected to the dual-motor power. Since the AM and TM are arranged in coaxial coupling through the transmission, the dual motor output torques are mutually additive and the speeds are proportionally consistent. In order to reduce the torsional vibration of the system, the motor power shaft and the system output shaft are arranged on the same straight line.

Since the TM is directly connected to the drive axle, which alone constitutes a conventional single motor system, the vehicle will not experience power interruption during operation, that is, the vehicle is driven by AM and TM in the torque coupling mode. During the gearshift process, the AM is separated from the system output shaft and the vehicle is driven solely by TM, which compensates for the torque loss induced by the lack of AM power.

B. DMCP SYSTEM MODELING

1) TRACTION MOTOR AND AUXILIARY MOTOR

The TM and AM are both permanent magnet synchronous motors (PMSM), Their dynamic characteristics can be expressed by establishing boundary constraints on the response rate of motors. The total efficiency of AM and TM can be modeled through a preset static map, as shown in Fig.2, which is obtained by experiment in prior. Thus, the efficiency and dynamics model of the motors can be described as follow [8]:

$$\begin{cases} P_{\mathrm{TM/AM}} = T_{\mathrm{TM/AM}} \cdot \omega_{\mathrm{TM/AM}} \cdot \eta_{\mathrm{TM/AM}}^{-\mathrm{sgn}(T_{\mathrm{TM/AM}} \cdot \omega_{\mathrm{TM/AM}})} \\ \mathrm{sgn}(T_{\mathrm{TM/AM}} \cdot \omega_{\mathrm{TM/AM}}) \\ \quad = \begin{Bmatrix} 1 & T_{\mathrm{TM/AM}} \cdot \omega_{\mathrm{TM/AM}} \geq 0 \\ -1 & T_{\mathrm{TM/AM}} \cdot \omega_{\mathrm{TM/AM}} < 0 \end{Bmatrix}, \left| \dfrac{dT_{\mathrm{TM/AM}}}{dt} \right| \\ \quad \leq k_{\mathrm{mot}} \end{cases} \tag{1}$$

where $P_{\mathrm{TM/AM}}$ represents the electric power of motor, $T_{\mathrm{TM/AM}}$ and $\omega_{\mathrm{TM/AM}}$ are the torque and rotation speed of the motors, respectively, and k_{mot} is an adjustable response gradient threshold. The motor efficiency η can be determined by a two-dimension lookup table according to the torque $T_{\mathrm{TM/AM}}$ and rotation speed $\omega_{\mathrm{TM/AM}}$.

2) TRANSMISSION MODEL

As shown in Fig.3, the transmission is a single planetary gearbox, and the transmission is divided into 2 gears. Under the action of the synchronizer, the transmission is in the first gear when the ring gear is fixedly connected to the planetary row housing, and the transmission ratio is 2.98 at this point; when the ring gear is fixedly connected to the planet carrier of the planetary row, the transmission ratio is 1. Transmission ratios of different gears can be expressed as:

$$i_{SP}^{C} = \frac{\omega_S^C}{\omega_P^C} = \frac{\omega_S - \omega_C}{\omega_P - \omega_C} = -\frac{z_P}{z_S} = -\frac{r_P}{r_S} \tag{2}$$

$$i_{SR}^{C} = \frac{\omega_S^C}{\omega_R^C} = \frac{\omega_S - \omega_C}{\omega_R - \omega_C} = -\frac{z_R}{z_S} = -\frac{r_R}{r_S} \tag{3}$$

where i_{SP}^{C} is the transmission radio between sun gear and planet gear; i_{SR}^{C} is the transmission radio between sun gear and ring; ω_P^C is the relative angular velocity of planet gear and carrier, ω_S^C is the relative angular velocity of sun gear and carrier, ω_R^C is the relative angular velocity of ring and carrier; $\omega_{\mathrm{P}}\omega_{\mathrm{S}}$ ω_{R} are the angular velocity of planet gear, sun gear and ring, respectively; z_{p}, z_{s},z_{R} are the teeth of planet gear, sun gear and ring, respectively; r_{P}, r_{S}, r_{R} are the reference radius of planet gear, sun gear and ring, respectively. According to geometric relations, following formula can be obtained:

$$\begin{cases} 2\omega_P r_P = \omega_R r_R - \omega_S r_S \\ 2\omega_C r_C = \omega_R r_R + \omega_S r_S \end{cases} \tag{4}$$

Finally, the kinematic equation of two-gear planetary transmission can be obtained:

$$\begin{bmatrix} \omega_P \\ \omega_C \end{bmatrix} = \begin{bmatrix} \dfrac{1}{-k_p+1} & \dfrac{k_p}{k_p-1} \\ \dfrac{1}{k_p+1} & \dfrac{k_p}{k_p+1} \end{bmatrix} \begin{bmatrix} \omega_S \\ \omega_R \end{bmatrix} \tag{5}$$

where k_{p} is the characteristic parameter, which is obtained by dividing teeth of ring by teeth of sun gear.

3) DYNAMICAL MODEL OF GEAR ENGAGEMENT

As the most important state of gearshift process, gear engagement directly determines the indicator of gearshift quality. It represents the movement process of the sleeve from neutral position to the target gear position. The most representative nodes of gear engagement are mechanical synchronization node and tooth contact node. Mechanical synchronization is the process in which sleeve pushes the synhronizer ring into contact with the friction cone to eliminate the speed difference. The dynamical function can be represented as:

$$J_{sla} \cdot \frac{d\omega_{sla}}{dt} = \frac{F_{msyn} \cdot \Delta i \cdot \mu_{msyn} \cdot (R_1 + R_2)}{\sin\alpha} - T_L^{eq}(\omega_{sla}) \tag{6}$$

where F_{msym} is the force of gearshift actuator in synchronization node; J_{sla} is the inertia of synchronized part; ω_{sla} is angular velocity of synchronized part; α is the friction cone surface angle; μ_{msym} is the friction coefficient of friction cone surface; R_1 and R_2 are effective radiuses of dual conical surfaces-generated synchronizer; $T_L^{eq}(\omega_{sla})$ is the resistance moment in process. The tooth contact node is the collision place of sleeve and target gear. The dynamical function can be represented as:

$$J_{sla} \cdot \frac{d\omega_{sla}}{dt} = F_{t\_EG} \cdot R_{cop} \cdot \Delta i - T_L^{eq}(\omega_{sla}) \tag{7}$$

FIGURE 1. The DMCP application scenario.

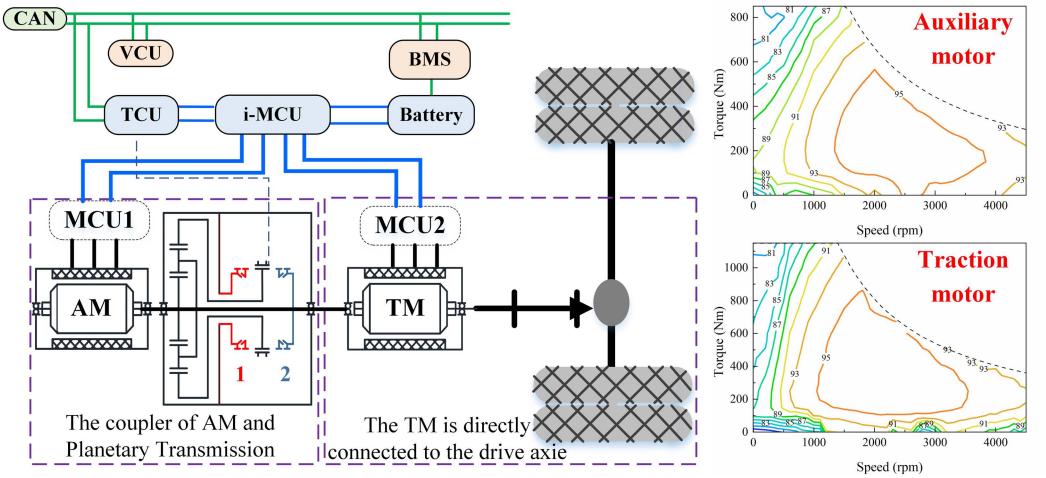

FIGURE 2. The scheme of DMCP system and Efficiency map of the motors.

where R_{cop} is the effective radius of spline in the sleeve; F_{t_EG} is the tangential force of gearshift actuator in process; Δi is the equivalent transmission ratio of synchronized part

III. GEARSHIFT CONTROL SYSTEM

In general, the control of vehicle powertrain system is executed in a hierarchical manner. The gearshift process is coordinated by the vehicle control unit (VCU) and transmission control unit (TCU) which monitors the control logic operating status.

The coordination gearshift control strategy of DMCP system is shown in Fig.4. This strategy is mainly comprised of following five stages Stage 1: Reduce AM torque to the threshold value and coordinate TM torque to maintain powertrain output torque; Stage2: Thrust the sleeve into the neutral position; Stage 3: Eliminate speed discrepancy of TM and AM; Stage4: Thrust the sleeve into the target gear position; Stage 5: Reinstate TM and AM torque to the target value. It should be also noted that the control mode of AM is switched according to the specific gearshift stage.

In general, gearshift faults often occur in the engagement stage. Since the influence of speed variation rate of output shaft on synchronization and tooth contact is ignored in the initial design of the gear shift strategy.

This paper reveals the failure of gearshift caused by oversized speed variation rate of output shaft. Then a robust tracking and disturbance suppression control method based on hierarchy layer LQR is proposed.

A. PROBLEM DESCRIPTION

In the experiment process, the PI closed-loop control which ignores the change of external load will lead to gearshift failure. As shown in Fig.5, the sleeve has been limited to a distance of 4 mm from the target gear position. At the same time, the maximum angular acceleration reached 12.2 rad/s^2.

The main reason of gearshift failure is the resistance torque generated by angular acceleration. As shown in Fig.1, the operating environment of the system is relatively complex, and the routes are mostly in the mountains and there are many

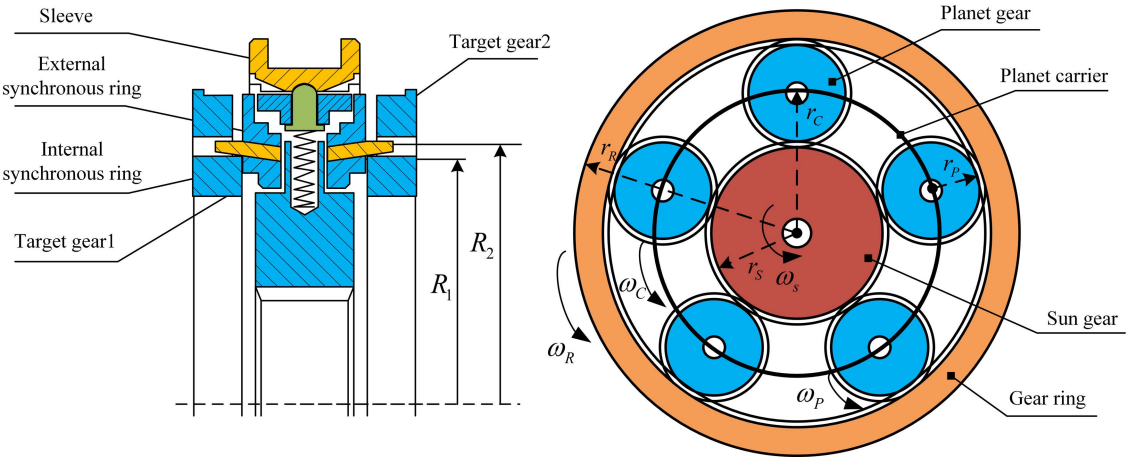

FIGURE 3. Single planetary gearbox.

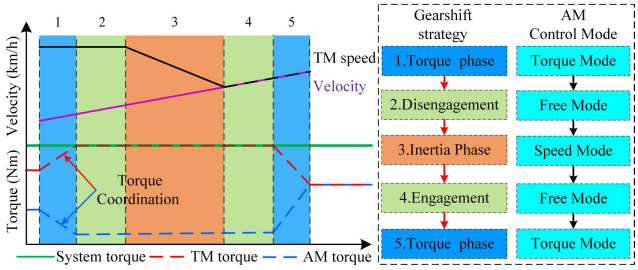

FIGURE 4. Gearshift strategy and AM control mode.

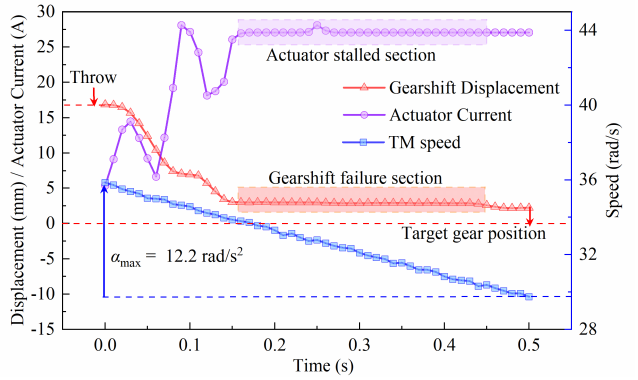

FIGURE 5. Experiment data of Gearshift failure.

ramps. Some slopes are relatively large, and the rotational speed of the output shaft may change greatly during the uphill or downhill process, which increases the risk of shifting failure during the shifting process.

The system load change directly reflects the acceleration value of the output shaft integrated with TM. Therefore, the suitable torque control curve of TM can effectively reduce the angular acceleration and avoid shifting failure in gearshift process.

B. CONTROL STRATEGY PROCESS

Aiming at poor system adaptation to external disturbances, this paper designs a controller to solve the complex robust tracking optimal control problem during gearshift process. The control flow is shown in Fig. 6, and a more detailed explanation will be given below. The disturbance observer needs to estimate the TM speed and the vehicle load torque. The vehicle load includes wind resistance, rolling resistance, slope resistance and mechanical braking torque.

Since the gearshift control process is a typical multi-input multi-output process, each output is solely controlled by a corresponding input in order to set an appropriate gearshift rule and make the input and output interrelated. A hierarchy LQR controller based on the system decoupling method is proposed. The disturbance terms and state variables of the superstratum and substratum controllers are coupled with each other. Taking as an example, the state variable x^{ul} of DSLQR controller is the estimated value of TM speed change rate $\dot{\hat{\omega}}_{TM}$, which is also the disturbance term of RTLQR controller.

1) DYNAMICAL EQUATION

The controlled objects in engagement process are gearshift actuator DCM and traction motor TM. When the charge rate of output shaft speed exceeds a range in engagement process, it will affect the gearshift quality or lead to gearshift failure, so it is necessary to control the torque of TM to reduce influence of the change rate of output shaft speed.

The goal of engagement process is to allow the synchronizer to contact with target gear quickly and accurately, achieving ''inter-tooth pairing''. At the same time, the relative angular velocity of the synchronizer and target gear is close to zero in the beginning of tooth contact process. Finally, it is necessary to control the change rate of output shaft speed as much as possible to reduce gearshift shock.

Further, the hierarchy LQR controller proposed is adopted to accomplish the mentioned control objectives, in which the superstratum is used to control the speed difference in tooth surface contact node; the substratum is used to realize the control of global TM speed change rate. The dual-layer controllers are coupled with each other, and the multi-layer

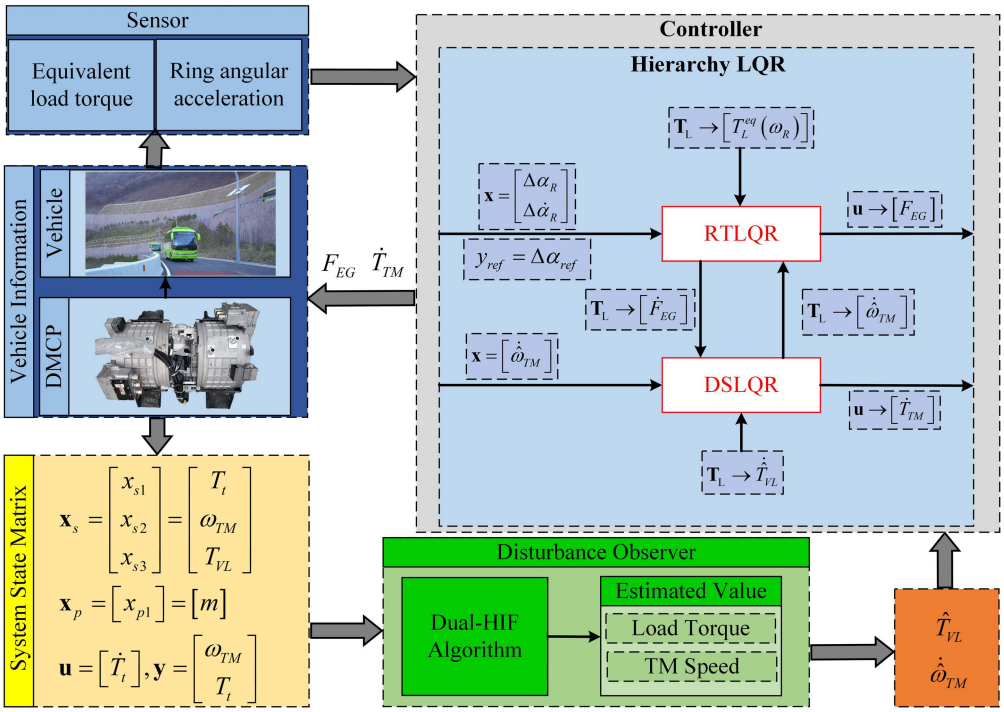

FIGURE 6. The process of gearshift strategy.

control system is realized through the decoupling between the output control quantity and input.

Under the hierarchy controller architecture, the dynamic function of the superstratum can be expressed as:

$$\Delta\ddot{\alpha}_R = \frac{R_{cop}}{J_R^{eq}} \frac{cos\left(\gamma_g/2\right) - \mu_{eg}\sin\left(\gamma_g/2\right)}{\sin\left(\gamma_g/2\right) + \mu_{eg}cos\left(\gamma_g/2\right)} F_{EG} - \frac{T_L^{eq}(\omega_R)}{J_R^{eq}} - \left(\frac{\zeta_j}{J_R^{eq}} + 1\right)\dot{\hat{\omega}}_{TM} \tag{8}$$

The dynamic function of the substratum can be expressed as:

$$\begin{cases} \dot{\hat{\omega}}_{TM} = k_{F_{EG}} F_{EG} + \dfrac{i_0^2}{\delta m r_T^2} T_{TM} + \dfrac{i_0}{\delta m r_T^2} \hat{T}_{VL} \\ k_{F_{EG}} = \varepsilon\,(gear) \cdot \mathrm{sgn}\left(\dot{\hat{\omega}}_{TM}\right) \\ \quad \times \dfrac{i_0^2 R_{cop}}{\delta m r_T^2} \dfrac{cos\left(\gamma_g/2\right) - \mu_{eg}\sin\left(\gamma_g/2\right)}{\sin\left(\gamma_g/2\right) + \mu_{eg}cos\left(\gamma_g/2\right)} \\ \varepsilon\,(gear) = \begin{cases} 0, & gear = 1 \\ 1, & gear = 2 \end{cases}, \\ \mathrm{sgn}\left(\dot{\hat{\omega}}_{TM}\right) = \begin{cases} -1, & \dot{\hat{\omega}}_{TM} > 0 \\ 1, & \dot{\hat{\omega}}_{TM} < 0 \end{cases} \\ \zeta_1 = \left[J_{21} + \dfrac{n_P k_P J_P}{(k_P - 1)^2}\right] \cdot (k_p + 1), \\ \zeta_2 = J_{21} + J_{22} - \dfrac{n_P k_p J_P}{k_p - 1} \end{cases} \tag{9}$$

where $\Delta\alpha_R$ is the relative rotation angle between synchronizer and output shaft; $\varepsilon\,(gear)$ indicates whether the impact caused by the synchronizing torque acts on the output shaft. In the first gear, the synchronizing torque acts on the transmission housing, which will not affect the vehicle impact. In the second gear, the synchronizing torque acts on the output shaft, which will affect the vehicle impact. R_{cop} is the effective radius of spline in sleeve; J_R^{eq} is the equivalent inertia of vehicle; γ_g is the spline kerf angle of sleeve; μ_{eg} is the friction coefficient on the tooth surface of sleeve and gear ring; F_{EG} is the gearshift force; $\dot{\hat{\omega}}_{TM}$ is the estimated value of TM speed change rate.

2) ROBUST TRACKING LQR CONTROLLER

The upper layer is robust tracking LQR, and its state space equation calibration formula is:

$$\begin{cases} \dot{\mathbf{x}}^{ul} = \mathbf{A}^{ul}\mathbf{x}^{ul} + \mathbf{B}^{ul}\mathbf{u}^{ul} + \mathbf{M}^{ul}\mathbf{d}^{ul} \\ \mathbf{y}^{ul} = \mathbf{C}^{ul}\mathbf{x}^{ul} \end{cases} \tag{10}$$

Define the state equation matrix under the controller:

$$\begin{cases} \mathbf{x}^{ul} = \begin{bmatrix} x_1^{ul} \\ x_2^{ul} \end{bmatrix} = \begin{bmatrix} \Delta\alpha_R \\ \Delta\dot{\alpha}_R \end{bmatrix}, \quad \mathbf{u}^{ul} = [F_{EG}] \\ \mathbf{d}^{ul} = \begin{bmatrix} T_L^{eq}(\omega_R) \\ \dot{\hat{\omega}}_{TM} \end{bmatrix}, \quad \mathbf{y}_{ref}^{ul} = \left[\Delta\alpha_{Rref}\right] \end{cases} \tag{11}$$

$$\begin{cases} \mathbf{A}^{ul} = \begin{bmatrix} 0 & 1 \\ 0 & 0 \end{bmatrix} \\ \mathbf{B}^{ul} = \begin{bmatrix} 0 \\ \dfrac{R_{cop}}{J_R^{eq}} \dfrac{cos\left(\gamma_g/2\right) - \mu_{eg} \sin\left(\gamma_g/2\right)}{\sin\left(\gamma_g/2\right) + \mu_{eg} cos\left(\gamma_g/2\right)} \end{bmatrix} \\ \mathbf{C}^{ul} = \begin{bmatrix} 1 & 0 \end{bmatrix}, \mathbf{M}^{ul} = \begin{bmatrix} -\dfrac{1}{J_R^{eq}} \\ -\dfrac{\zeta_j + J_R^{eq}}{J_R^{eq}} \end{bmatrix} \end{cases} \tag{12}$$

The upper layer control optimization problem of gear pair gear can be described as:

$$\min_{\mathbf{x}^{ul}(t), \mathbf{u}^{ul}(t)} J^{ul} = \frac{1}{2} \int_{t_0}^{t_f} \left[\mathbf{e}^{\mathbf{T}} \mathbf{Q}^{ul} \mathbf{e} + \left(\mathbf{u}^{ul}\right)^{\mathbf{T}} \mathbf{R}^{ul} \mathbf{u}^{ul} \right] dt \tag{13}$$

where $\mathbf{Q}^{ul}$ is the weight coefficient matrix of tracking error and $\mathbf{R}^{ul}$ is the weight coefficient matrix of control variable:

$$\mathbf{e} = \mathbf{y}_{ref} - \mathbf{y}^{ul} = \left[\frac{\pi}{2N} - \Delta\alpha_R \right] \tag{14}$$

$$\mathbf{Q}^{ul} = \begin{bmatrix} Q_1^{ul} & 0 \\ 0 & Q_2^{ul} \end{bmatrix}, \quad \mathbf{R}^{ul} = \left[R_1^{ul} \right] \tag{15}$$

Hamiltonian function is constructed to solve LQR standard form problem:

$$\begin{aligned} \mathbf{H}^{ul} = \frac{1}{2} \Big[& \left(\mathbf{y}_{ref} - \mathbf{C}^{ul} \mathbf{x}^{ul}\right)^{\mathbf{T}} \mathbf{Q}^{ul} \left(\mathbf{y}_{ref} - \mathbf{C}^{ul} \mathbf{x}^{ul}\right) \\ & + \left(\mathbf{u}^{ul\mathbf{T}}\right) \mathbf{R}^{ul} \mathbf{u}^{ul} \Big] + \boldsymbol{\lambda}^{ul} \left(\mathbf{A}^{ul} \mathbf{x}^{ul} + \mathbf{B}^{ul} \mathbf{u}^{ul} + \mathbf{M}^{ul} \mathbf{d}^{ul}\right) \end{aligned} \tag{16}$$

Multiplier function matrix:

$$\boldsymbol{\lambda}^{ul} = \mathbf{P}^{ul} \mathbf{x}^{ul} - \mathbf{g}^{ul} + \mathbf{N}_0^{ul} \mathbf{d}^{ul} + \sum_{i=1}^{n} \mathbf{N}_i^{ul} \left(\mathbf{d}^{ul}\right)^{(i)} \tag{17}$$

$\mathbf{g}^{ul}$ is the gain matrix of $\mathbf{y}^{ul}$, $\mathbf{d}^{ul}$ is the disturbance of the system.$\mathbf{N}_0^{ul}$ is the constant coefficient matrix of $\mathbf{d}^{ul}$, $\left(\mathbf{d}^{ul}\right)^{(i)}$ is i-th derivative of $\mathbf{d}^{ul}$, $\mathbf{N}_i^{ul}$ is the constant coefficient matrix of $\left(\mathbf{d}^{ul}\right)^{(i)}$, n is the highest order derivative of disturbance. In this paper, the highest order derivative is 1st.

$\mathbf{P}^{ul}$ is solved by Riccati equation:

$$\begin{aligned} & \mathbf{P}^{ul} \mathbf{A}^{ul} - \mathbf{P}^{ul} \mathbf{B}^{ul} \left(\mathbf{R}^{ul}\right)^{-1} \left(\mathbf{B}^{ul}\right)^{\mathbf{T}} \mathbf{P}^{ul} \\ & + \left(\mathbf{C}^{ul}\right)^{\mathbf{T}} \mathbf{Q}^{ul} \mathbf{C}^{ul} + \left(\mathbf{A}^{ul}\right)^{\mathbf{T}} \mathbf{P}^{ul} = \mathbf{0} \end{aligned} \tag{18}$$

According to the derivation:

$$\begin{cases} \mathbf{N}_0^{ul} = \left[\mathbf{P}^{ul} \mathbf{B}^{ul} \left(\mathbf{R}^{ul}\right)^{-1} \left(\mathbf{B}^{ul}\right)^{\mathbf{T}} - \left(\mathbf{A}^{ul}\right)^{\mathbf{T}} \right]^{-1} \\ \quad \times \mathbf{P}^{ul} \mathbf{M}^{ul} \\ \mathbf{N}_i^{ul} = \left[\mathbf{P}^{ul} \mathbf{B}^{ul} \left(\mathbf{R}^{ul}\right)^{-1} \left(\mathbf{B}^{ul}\right)^{\mathbf{T}} - \left(\mathbf{A}^{ul}\right)^{\mathbf{T}} \right]^{-1} \\ \quad \times \mathbf{N}_{i-1}^{ul}, i = 1, 2, \cdots \\ \mathbf{g}^{ul} = \left[\mathbf{P}^{ul} \mathbf{B}^{ul} \left(\mathbf{R}^{ul}\right)^{-1} \left(\mathbf{B}^{ul}\right)^{\mathbf{T}} - \left(\mathbf{A}^{ul}\right)^{\mathbf{T}} \right]^{-1} \\ \quad \times \left(\mathbf{C}^{ul}\right)^{\mathbf{T}} \mathbf{Q}^{ul} \mathbf{y}_{ref} \end{cases} \tag{19}$$

When designing the optimal controller for the engagement process, the derivative of the disturbance adopts the first-order derivative, and the optimal control law for the engagement process is:

$$\begin{cases} \left(\mathbf{u}^{ul}\right)^{*} = \mathbf{K}_{\mathbf{x}^{ul}} \begin{bmatrix} \Delta\alpha_R \\ \Delta\dot{\alpha}_R \end{bmatrix} + \mathbf{K}_{\mathbf{y}_{ref}} \left[\dfrac{\pi}{2N} \right] \\ \quad + \mathbf{K}_{\mathbf{d}^{ul}} \begin{bmatrix} T_L^{eq}(\omega_R) \\ \dot{\hat{\omega}}_{TM} \end{bmatrix} + \mathbf{K}_{\mathbf{d}_1^{ul}} \begin{bmatrix} T_L^{eq}(\omega_R) \\ \dot{\hat{\omega}}_{TM} \end{bmatrix}' \\ \mathbf{K}_{\mathbf{x}^{ul}} = -\left(\mathbf{R}^{ul}\right)^{-1} \left(\mathbf{B}^{ul}\right)^{\mathbf{T}} \mathbf{P}^{ul} \\ \mathbf{K}_{\mathbf{y}_{ref}} = \left(\mathbf{R}^{ul}\right)^{-1} \left(\mathbf{B}^{ul}\right)^{\mathbf{T}} \\ \quad \times \left[\mathbf{P}^{ul} \mathbf{B}^{ul} \left(\mathbf{R}^{ul}\right)^{-1} \left(\mathbf{B}^{ul}\right)^{\mathbf{T}} - \left(\mathbf{A}^{ul}\right)^{\mathbf{T}} \right]^{-1} \left(\mathbf{C}^{ul}\right)^{\mathbf{T}} \mathbf{Q}^{ul} \\ \mathbf{K}_{\mathbf{d}^{ul}} = -\left(\mathbf{R}^{ul}\right)^{-1} \left(\mathbf{B}^{ul}\right)^{\mathbf{T}} \mathbf{N}_0^{ul} \\ \mathbf{K}_{\mathbf{d}_1^{ul}} = -\left(\mathbf{R}^{ul}\right)^{-1} \left(\mathbf{B}^{ul}\right)^{\mathbf{T}} \mathbf{N}_1^{ul} \end{cases} \tag{20}$$

3) DISTURBANCE SUPPRESSION LQR CONTROLLER

The lower layer is disturbance suppression LQR, and its state space equation calibration formula is:

$$\begin{cases} \dot{\mathbf{x}}^{dl} = \mathbf{A}^{dl} \mathbf{x}^{dl} + \mathbf{B}^{dl}\ \mathbf{u}^{dl} + \mathbf{M}^{dl} \mathbf{d}^{dl} \\ \mathbf{y}^{dl} = \mathbf{C}^{dl} \mathbf{x}^{dl} \end{cases} \tag{21}$$

Define the state equation matrix under the controller (22) and (23), as shown at the bottom of the next page.

The lower layer control optimization problem of gear pair gear can be described as:

$$\min_{\mathbf{x}^{dl}(t), \mathbf{u}^{dl}(t)} J^{dl} = \frac{1}{2} \int_{t_0}^{t_f} \left[\left(\mathbf{x}^{dl}\right)^{\mathbf{T}} \mathbf{Q}^{dl} \mathbf{x}^{dl} + \left(\mathbf{u}^{dl}\right)^{\mathbf{T}} \mathbf{R}^{dl} \mathbf{u}^{dl} \right] dt \tag{24}$$

where $\mathbf{Q}^{dl}$ is the weight coefficient matrix of tracking error and $\mathbf{R}^{dl}$ is the weight coefficient matrix of control variable:

$$\begin{cases} \mathbf{Q}^{dl} = \left[Q_1^{dl} \right] \\ \mathbf{R}^{dl} = \left[R_1^{dl} \right] \end{cases} \tag{25}$$

Hamiltonian function is constructed:

$$\mathbf{H}^{dl} = \frac{1}{2}\left[\left(\mathbf{x}^{dl}\right)^{\mathbf{T}}\mathbf{Q}^{dl}\mathbf{x}^{dl} + \left(\mathbf{u}^{dl}\right)^{\mathbf{T}}\mathbf{R}^{dl}\mathbf{u}^{dl}\right] + \boldsymbol{\lambda}^{dl}\left(\mathbf{A}^{dl}\mathbf{x}^{dl} + \mathbf{B}^{dl}\mathbf{u}^{dl} + \mathbf{M}^{dl}\mathbf{d}^{dl}\right) \tag{26}$$

Determine the optimal control law according to extreme conditions:

$$\frac{\partial \mathbf{H}^{dl}}{\partial \mathbf{u}^{dl}} = 0 \Rightarrow \left(\mathbf{u}^{dl}\right)^{*} = -\left(\mathbf{R}^{dl}\right)^{-1}\left(\mathbf{B}^{dl}\right)^{\mathbf{T}}\boldsymbol{\lambda}^{dl} \tag{27}$$

Multiplier function matrix:

$$\boldsymbol{\lambda}^{dl} = \mathbf{P}^{dl}\mathbf{x}^{dl} + \mathbf{N}_0^{dl}\mathbf{d}^{dl} + \sum_{i=1}^{n}\mathbf{N}_i^{dl}\left(\mathbf{d}^{dl}\right)^{(i)} \tag{28}$$

$\mathbf{d}^{dl}$ is the disturbance of the system. $\mathbf{N}_0^{dl}$ is the constant coefficient matrix of $\mathbf{d}^{dl}$, $\left(\mathbf{d}^{dl}\right)^{(i)}$ is i-th derivative of $\mathbf{d}^{dl}$, $\mathbf{N}_i^{dl}$ is the constant coefficient matrix of $\left(\mathbf{d}^{dl}\right)^{(i)}$, n is the highest order derivative of disturbance. In this paper, the highest order derivative is 1st.

Parameter matrix:

$$\begin{cases} \mathbf{N}_0^{dl} = \left[\mathbf{P}^{dl}\mathbf{B}^{dl}\left(\mathbf{R}^{dl}\right)^{-1}\left(\mathbf{B}^{dl}\right)^{\mathbf{T}} - \left(\mathbf{A}^{dl}\right)^{\mathbf{T}}\right]^{-1} \\ \quad \times \mathbf{P}^{dl}\mathbf{M}^{dl} \\ \mathbf{N}_i^{dl} = \left[\mathbf{P}^{dl}\mathbf{B}^{dl}\left(\mathbf{R}^{dl}\right)^{-1}\left(\mathbf{B}^{dl}\right)^{\mathbf{T}} - \left(\mathbf{A}^{dl}\right)^{\mathbf{T}}\right]^{-1} \\ \quad \times \mathbf{N}_{i-1}^{dl},\ i = 1, 2, \cdots \end{cases} \tag{29}$$

The optimal control law:

$$\begin{cases} \left(\mathbf{u}^{dl}\right)^{*} = \mathbf{K}_{\mathbf{x}^{dl}}\left[\dot{\hat{\omega}}_{TM}\right] + \mathbf{K}_{\mathbf{d}^{dl}}\begin{bmatrix}\dot{F}_{EG} \\ \dot{\hat{T}}_{VL}\end{bmatrix} + \mathbf{K}_{\mathbf{d}_1^{dl}}\begin{bmatrix}\dot{F}_{EG} \\ \dot{\hat{T}}_{VL}\end{bmatrix}' \\ \mathbf{K}_{\mathbf{x}^{dl}} = -\mathbf{B}^{dl}\left(\mathbf{R}^{dl}\right)^{-1}\mathbf{P}^{dl} \\ \mathbf{K}_{\mathbf{d}^{dl}} = -\mathbf{B}^{dl}\left(\mathbf{R}^{dl}\right)^{-1}\mathbf{N}_0^{dl} \\ \mathbf{K}_{\mathbf{d}_1^{dl}} = -\mathbf{B}^{dl}\left(\mathbf{R}^{dl}\right)^{-1}\mathbf{N}_1^{dl} \end{cases} \tag{30}$$

IV. SIMULATION AND COMPARISON

This section mainly analyzes the engagement process. Firstly, the hierarchical LQR controller proposed in this paper was simulated, and the influence of the hierarchical LQR controller with and without anti-disturbance on the gearshift process was compared; then the optimal control methods based on PI and variational method were comparatively analyzed. The simulation results showed that the hierarchical LQR control method proposed improved the gearshift quality. The system exhibited relatively good stability even in the presence of external interference.

The evaluation indicators include the completion gearshift, impact and the power loss rate. Generally, define the derivative of acceleration as impact:

$$j_x = \frac{da}{dt} = \frac{d\alpha}{dt} \tag{31}$$

$$j_V = \frac{d\left(\frac{d\omega_{TM}}{dt}\right)}{dt} \cdot \frac{r_T}{i_0} \tag{32}$$

For the dual-motor system studied in this paper, the power loss rate of the system k_{ploss} during the shifting process is at $[0, k]$, and there is no complete power interruption state. The definition of k is as follows:

$$\begin{cases} k_{Ploss} = \dfrac{T_{Req} - T_{out}}{T_{Req}} \times 100\% \\ k_{ploss} \in [0, k] \\ k = \dfrac{T_{Req} - T_{TM}}{T_{Req}} \times 100\% \end{cases} \tag{33}$$

A. SIMULATION RESULTS OF HLQR CONTROLLER

This section uses different weight coefficient matrices to simulate and analyze the gearshift process based on the designed hierarchical LQR controller. The upper layer controller selects a fixed weight coefficient, and the lower layer controller adjusts the weight coefficient of the TM motor torque to adjust the output shaft speed. The influence of the change rate of the output shaft speed on the shift performance is verified.

The following two sets of coefficient matrices are adopted in the simulation process:

$$\mathbf{x}^{dl} = \left[x_1^{dl}\right] = \left[\dot{\hat{\omega}}_{TM}\right],\quad \mathbf{u}^{dl} = \left[\dot{T}_{TM}\right],\ \mathbf{d}^{dl} = \begin{bmatrix}\dot{F}_{EG} \\ \dot{\hat{T}}_{VL}\end{bmatrix} \tag{22}$$

$$\begin{cases} \mathbf{A}^{dl} = [0], \mathbf{B}^{dl} = \left[\dfrac{i_0^2}{\delta m r_T^2}\right], \mathbf{C}^{dl} = [1] \\ \mathbf{M}^{dl} = \left[\varepsilon\,(gear)\cdot \operatorname{sgn}\left(\dot{\hat{\omega}}_{TM}\right)\dfrac{i_0^2 R_{cop}}{\delta m r_T^2}\dfrac{cos\left(\gamma_g/2\right) - \mu_{eg}\sin\left(\gamma_g/2\right)}{\sin\left(\gamma_g/2\right) + \mu_{eg}cos\left(\gamma_g/2\right)} \quad \dfrac{i_0}{\delta m r_T^2}\right] \end{cases} \tag{23}$$

Coefficient matrix group (1):
Upper layer:

$$\begin{cases} \mathbf{Q}^{ul} = \begin{bmatrix} 10^7 & 0 \\ 0 & 10 \end{bmatrix}, \mathbf{R}^{ul} = [1], \\ \mathbf{K}_{\mathbf{x}^{ul}} = \begin{bmatrix} -3162.3 & -316.8 \end{bmatrix} \\ \mathbf{K}_{\mathbf{y}_{ref}} = \begin{bmatrix} 3162.2 & 0 \end{bmatrix}, \mathbf{K}_{\mathbf{d}^{ul}} = [24.5949]\, \mathbf{K}_{\mathbf{d}_1^{ul}} = [0] \end{cases} \tag{34}$$

Lower layer:

$$\begin{cases} \mathbf{Q}^{dl} = [1000], \mathbf{R}^{dl} = [1], \mathbf{K}_{\mathbf{x}^{dl}} = [-31.6228] \\ \mathbf{K}_{\mathbf{d}^{dl}} = \begin{bmatrix} -0.243 & -0.1951 \end{bmatrix}, \\ \mathbf{K}_{\mathbf{d}_1^{dl}} = \begin{bmatrix} -1.1538 & -0.9264 \end{bmatrix} \end{cases} \tag{35}$$

Coefficient matrix group (2):
Upper layer:

$$\begin{cases} \mathbf{Q}^{ul} = \begin{bmatrix} 10^7 & 0 \\ 0 & 10 \end{bmatrix}, \mathbf{R}^{ul} = [1], \\ \mathbf{K}_{\mathbf{x}^{ul}} = \begin{bmatrix} -3162.3 & -316.8 \end{bmatrix} \\ \mathbf{K}_{\mathbf{y}_{ref}} = \begin{bmatrix} 3162.2 & 0 \end{bmatrix}, \mathbf{K}_{\mathbf{d}^{ul}} = [24.5949], \mathbf{K}_{\mathbf{d}_1^{ul}} = [0] \end{cases} \tag{36}$$

Lower layer:

$$\begin{cases} \mathbf{Q}^{dl} = [50000], \mathbf{R}^{dl} = [1], \mathbf{K}_{\mathbf{x}^{dl}} = [-223.6068] \\ \mathbf{K}_{\mathbf{d}^{dl}} = \begin{bmatrix} -0.243 & -0.1951 \end{bmatrix}, \\ \mathbf{K}_{\mathbf{d}_1^{dl}} = \begin{bmatrix} -0.1632 & -0.131 \end{bmatrix} \end{cases} \tag{37}$$

Simulation results are shown in Fig7-Fig11:

As shown in the simulation results, when the coefficient matrix (1) is used for optimal control, the speed change rate of the output shaft is large, and the speed change of the output shaft is fast. The negative torque generated is superimposed on the output shaft. Since the gearshift force produces a relatively small negative torque, the system output torque is basically equivalent to the TM torque. The shift force at terminal of shift process is about 120N, the maximum impact [absolute value] of the vehicle during the process is about -0.55m/s^3, and the maximum average power loss rate of the whole vehicle is about 28.74%. The coefficient matrix (2) increases the weighting factor of the speed change rate of the output shaft. The speed change rate of the output shaft decreases rapidly in the gearshift process, and the speed change rate of the output shaft is relatively slow. The shift force at terminal of shift process is about 60N, the maximum impact [absolute value] of the vehicle during the process is about -1.26m/s^3, and the maximum average power loss rate of the whole vehicle is about 44%. Table 1 lists the gearshift performance indicators based on coefficient matrix.

It can be seen from the simulation that the speed change rate of the output shaft is an important factor affecting the gear-to-tooth process. The greater the speed change rate of the output shaft, the greater the average Gear-shifting force. At a certain level, the gear-shifting force may exceed the limit of the actuator, causing the failure of gear-shifting. In addition, in the process of balancing the speed change rate of the output shaft, the shift quality was improved, but the change of output shaft torque occurred, resulting in the shock and power loss of the entire vehicle.

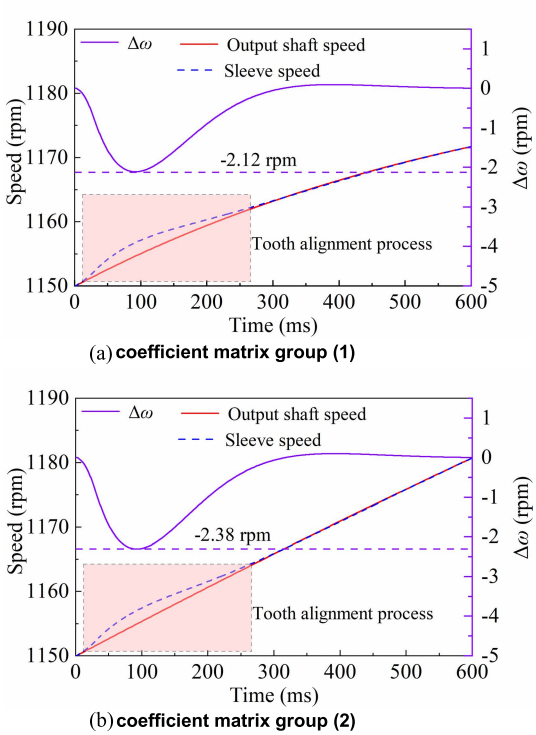

FIGURE 7. Speed variation curves of different coefficient matrices in engagement process.

B. METHOD COMPARISON

In the presence of external disturbances, the effect of hierarchy LQR with and without disturbance rejection on gearshift quality was comparatively analyzed through simulation. The simulation results are shown in Fig12-14. When the controller is equipped with disturbance rejection, the gearshift actuator can make synchronizer turn an angle quickly, and the engagement ring gear with the target gear achieves the effect of "tooth tip to tooth groove," realizing rapid shifting; when the controller does not have anti-disturbance function, the gear is engaged by using the same control parameters. In this case, the synchronizer rotated through a negative angle, which is a typical axial retreat phenomenon of the synchronizer. The gearshift force during gear shifting is small, and the synchronizer cannot rotate through the target angle to achieve "tooth tip pairing Cogging", which eventually leads to the failure of gear pairing. From the simulation results, it can be seen that in the presence of external disturbances, the designed hierarchy LQR controller has better robustness.

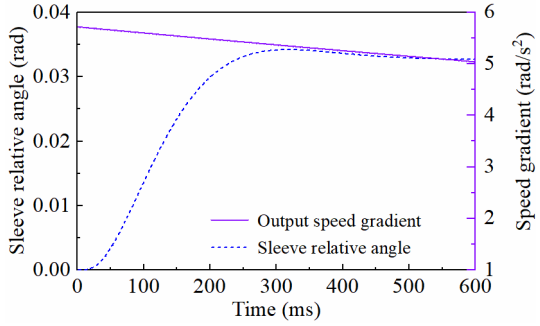

(a) coefficient matrix group (1)

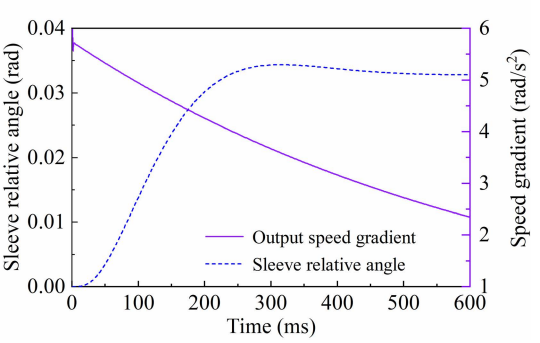

(b) coefficient matrix group (2)

FIGURE 8. Synchronizer angle variation curves of different coefficient matrices in engagement process.

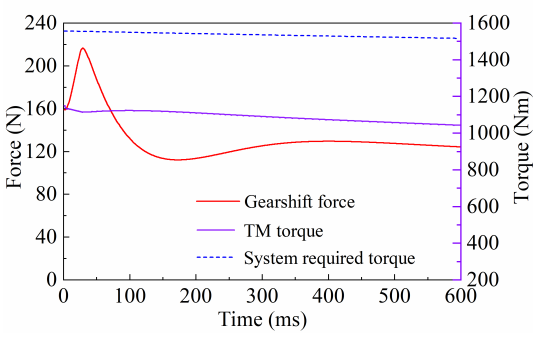

(a) coefficient matrix group (1)

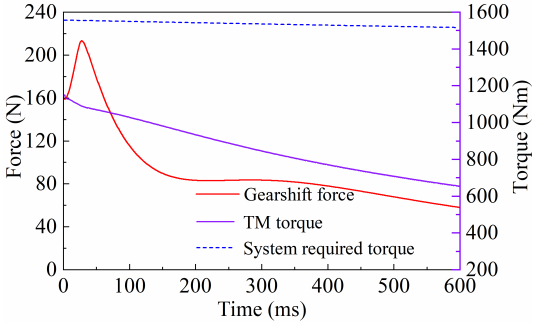

(b) coefficient matrix group (2)

FIGURE 9. Variation curves of shift force and torque of different coefficient matrices in engagement process.

Fig.15 shows the comparison curve of vehicle's impact degree in engagement process with three different algorithms. The shifting comfort based on HLQR algorithm is the best, the average impact degree is the lowest, and the maximum impact degree is -2.76m/s^3.Shifting comfort based on optimal control based on variational method (OCVM) algorithm takes the second place, with the maximum impact of $-4.32\ \text{m/s}^3$. The PI algorithm has the worst shifting comfort, with maximum impact degree of -4.95m/s^3, and the impact is bidirectional. The longest duration of the whole engagement process based on PI algorithm is 265ms, followed by the second shift time based on HLQR algorithm (210ms), and the shift time based on OCVM algorithm is the shortest (184ms).

Simulation results show that the HLQR algorithm proposed in this paper has better performance than the other two algorithms in improving the comprehensive shifting performance in the engagement process.

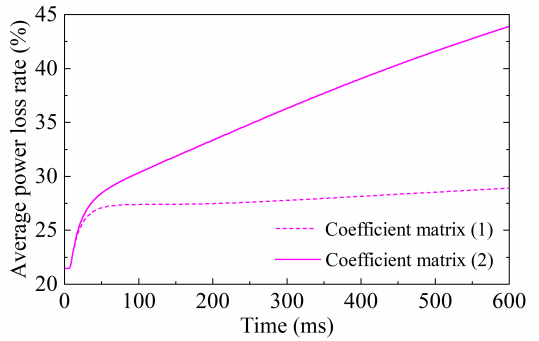

FIGURE 10. Average power loss rate of different coefficient matrix.

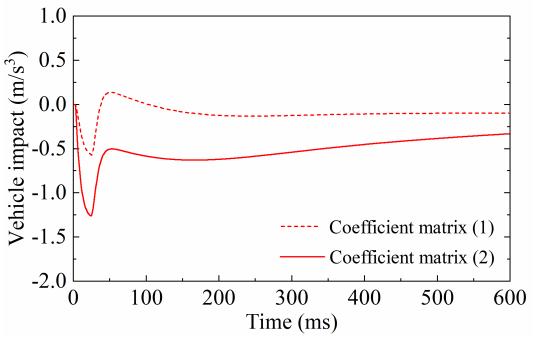

FIGURE 11. Vehicle impact of different coefficient matrix.

V. EXPERIENCE RESULTS

A. TEST PLATFORM

To verify the effectiveness of the control strategy designed in this paper, a test bench was built, as shown in Fig.16. Based on the control strategy designed in this paper, the shift test was carried out, and the tests results were compared with the results obtained by using other control algorithms. The test bench includes drive system (main motor, auxiliary motor, transmission, shift actuator, and transmission controller), high-voltage power supply, permanent magnet synchronous motor controller, load system (inertia tablets). The high-voltage power supply system provides a power source for the entire drive system, the permanent magnet

TABLE 1. Gearshift performance indicators of different coefficient matrix.

	Maximum vehicle impact [absolute value] [m/s^3]	Maximum average power loss rate [%]	Shift force at terminal of shift process [N]
coefficient matrix (1)	-0.55	28.74	120
coefficient matrix (2)	-1.26	44	60

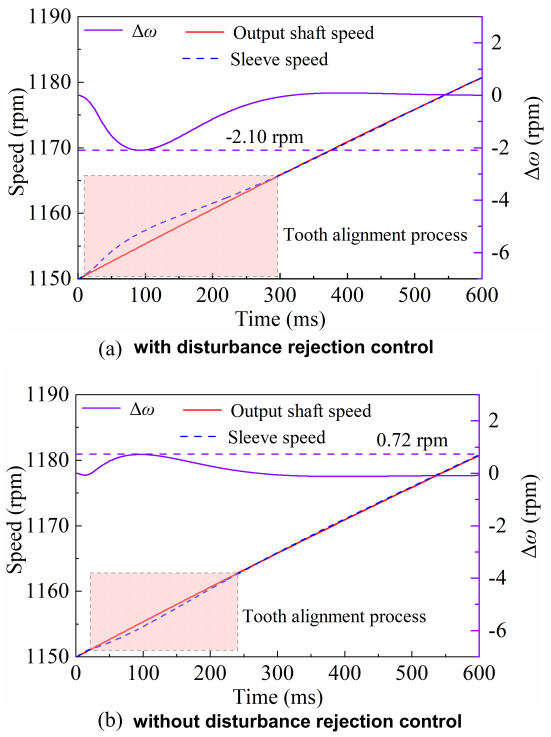

FIGURE 12. Variation curves of speed with and without disturbance rejection control in engagement process.

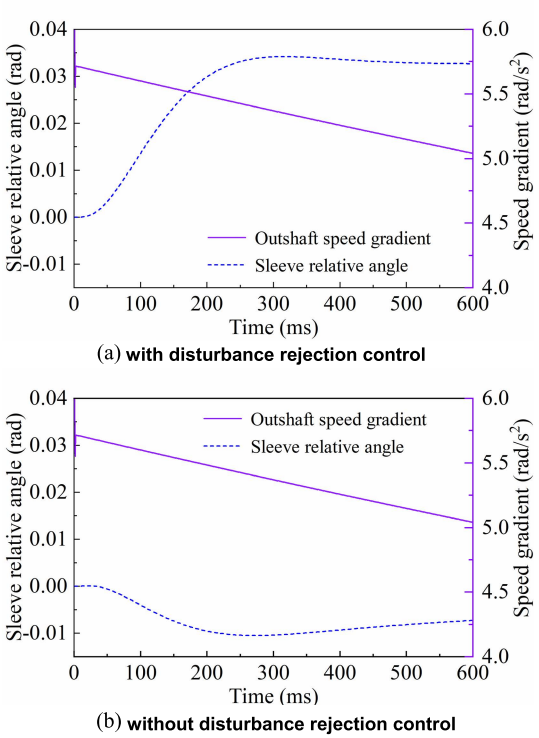

FIGURE 13. Variation curves of Sleeve Angle and output shaft speed gradient with and without disturbance rejection control in engagement process.

synchronous motor controller follows the upper layer (TCU) control instruction to control the output torque of the main motor and auxiliary motor, implement the motor speed acquisition and motor torque calculation, adjust the speed of the auxiliary motor in the shift process, thus realizing the cooperative control of the shift process. The load system provides the load for the whole drive system, The main motor and auxiliary motor output power for the power system as executive components. the transmission realizes the variable speed and variable torque of the drive. The shift actuator implements and responds to the shift command to shift the transmission.

Transmission Control Unit (TCU) is the main carrier to realize the control strategy designed in this paper. Fig.17 shows an overview of the hardware resources of the Transmission Control Unit (TCU). The microcontroller of TCU is Infineon TC234 chip, which is a 32-bit platform. The external crystal frequency is 20MHz, and the TCU hardware bus can be multiplied to 100MHz, which is rich enough to support complex algorithms.

Fig.18 is the network topology and data flow of the whole system. The main and auxiliary motor controllers transmit the processed torque and speed information to the transmission controller through CAN2. The transmission controller collects the electric current information and position information of the shift actuator, and calculates the corresponding shift force and DC motor speed. In order to analyze the performance of the designed control strategy more accurately, the transmission controller sets up a high frequency data acquisition module with the acquisition frequency of 10kHz, so that the data in the gearshift process can be stored in Flash first, and the data collected by high frequency can be sent to the PC via CAN1 after the shift process is completed.

B. TEST DATA ANALYSIS

In this section the influence of control strategies based on the hierarchical LQR and PI algorithms on the performance of engagement process is comparatively analyzed.

Fig.19 shows the torque curve of the output shaft during upshift process, in which the blue dotted line represents the situation when the target torque of the system is 300Nm. The torque of output shaft based on hierarchical LQR algorithm decreases smoothly from 300Nm to 85Nm. In contrast, the torque of the output shaft based on the PI algorithm fluctuates rapidly in the first 100ms, which is the main source of system impact, and then gradually decreases to 163Nm. Fig.20 shows

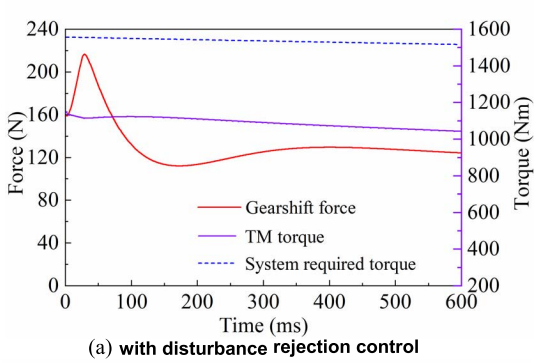

(a) with disturbance rejection control

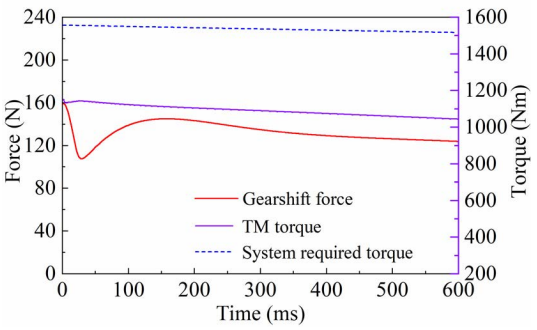

(b) without disturbance rejection control

FIGURE 14. Variation curves of drive system torque and gear-shifting force with and without disturbance rejection control in engagement process.

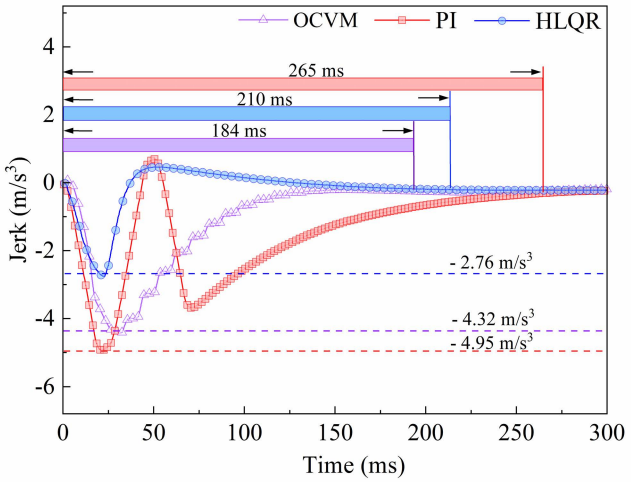

FIGURE 15. Comparison curves of vehicle's impact degree with different algorithms in engagement process.

the curve of output shaft speed during engagement process, the output torque based on the two different algorithms shows little difference in the first 100ms, and after that, the speed difference between them becomes larger and larger. During the whole gearing process, the output shaft speed based on hierarchical LQR algorithm increases from 898rpm to 945rpm, with an increment of 47rpm, and the output shaft speed based on PI algorithm increases from 905rpm to 1000rpm, with an increment of 95rpm.

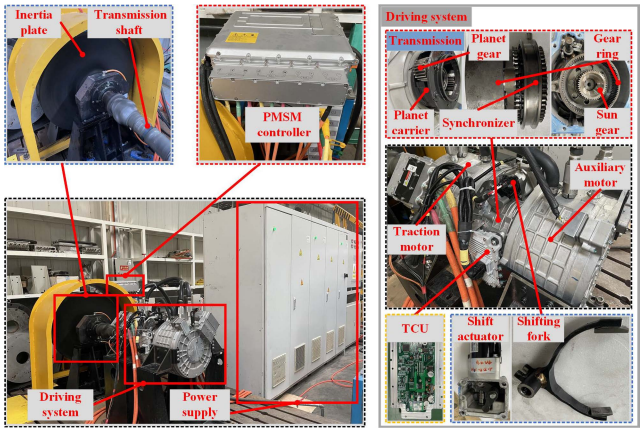

FIGURE 16. Test platform.

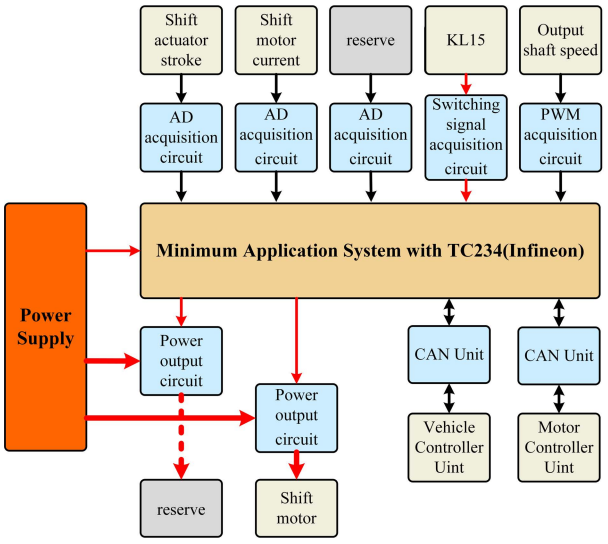

FIGURE 17. Overview of the hardware resources of the TCU.

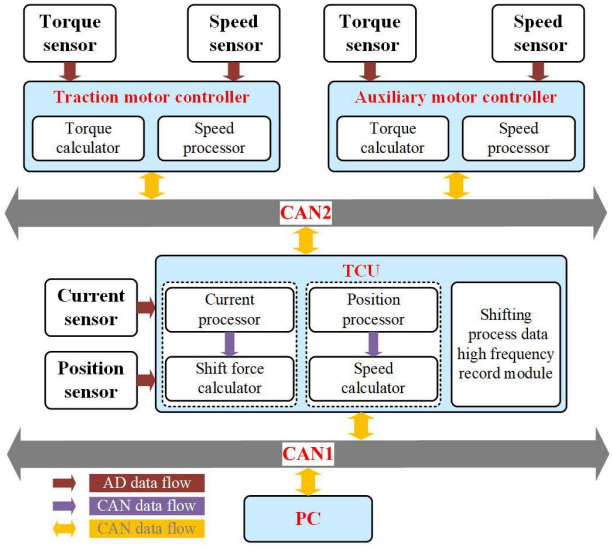

FIGURE 18. Bench system network topology and data flow.

Fig.21 shows the speed curve of the gearshift motor during engagement process. The average speed of shift motor based

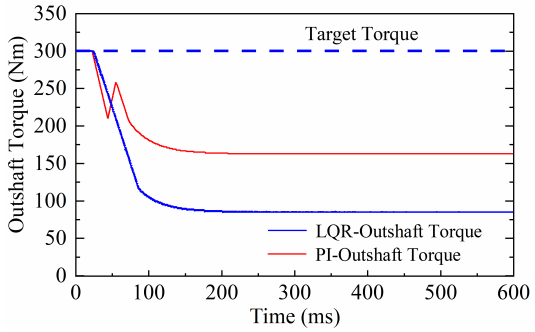

FIGURE 19. Torque curve of output shaft in engagement process.

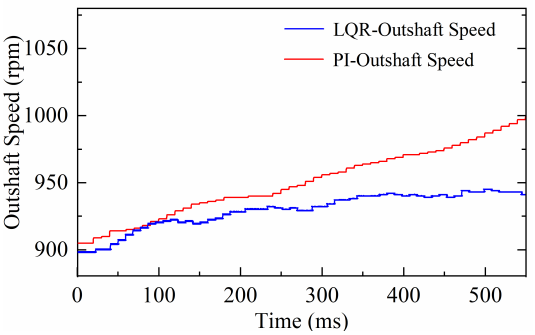

FIGURE 20. Speed curve of output shaft in engagement process.

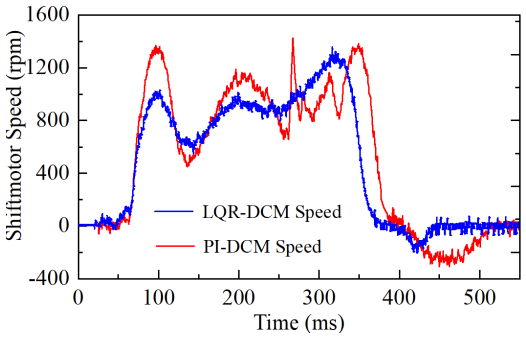

FIGURE 21. Speed curve of shift motor in engagement process.

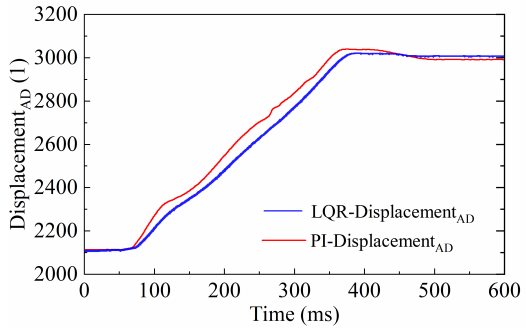

FIGURE 22. Displacement curve in engagement process.

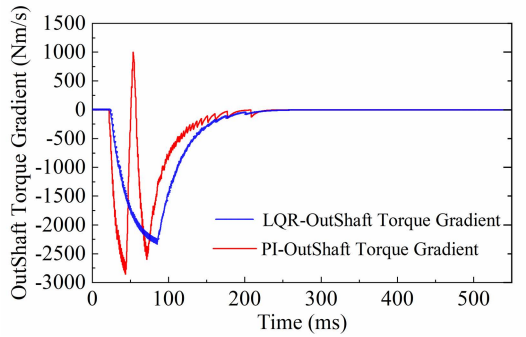

FIGURE 23. Torque gradient curve of output shaft in engagement process.

on PI algorithm is greater than that based on hierarchical LQR algorithm. Moreover, it can be seen that the speed of the shift motor based on PI algorithm fluctuates greatly due to the complex and random load received by the synchronizer during the upshift process, which shows that the stability of PI algorithm is not so good as hierarchical LQR algorithm.

Fig.22 shows the displacement curve of synchronizer during engagement process. The displacement is AD value, a synchronizer displacement of 1mm corresponds to an AD value of 60. The position of synchronizer based on PI algorithm reaches the target position faster than that based on hierarchical LQR algorithm. The positions of the synchronizers based the two algorithms are both overshoot between 350 and 400ms, but the displacement overshoot of synchronizer based on PI algorithm is greater. Combined with Fig.25, in fact, the shift force has been removed at about 400ms, but the synchronizer displacement in Fig.22 rebounds after 400ms. This is because the actuator and synchronizer are non-rigid bodies and there is a mechanical gap. Sudden unloading of the extrusion force is bound to cause a certain rebound of the synchronizer displacement, which explains why there is a negative speed of the shift motor after 400ms as shown in Fig.21.

Fig.23 $\sim$ Fig.25 show several key performance index curves. Fig.23 shows the curve of impact with respect to output shaft torque change rate. The maximum output shaft torque change rate based on hierarchical LQR algorithm and PI algorithm is -2331Nm/s and -2884Nm/s, respectively. Compared with PI algorithm, the torque change rate of output shaft based on hierarchical LQR algorithm is reduced by 19.17%. The impact based on hierarchical LQR algorithm is one-way impact, and the impact based on PI algorithm is two-way impact, so gearshift comfort based on PI algorithm is worse than that based on hierarchical LQR algorithm. Fig.24 shows the power loss rate (K_{ploss}) of the system during engagement process. The total target torque of the system is 300Nm, the maximum power loss rate based on hierarchical LQR algorithm is 71.67%, and the maximum power loss rate based on PI algorithm is 45.67%

Fig.25 shows the shift force curve during the shift process. The maximum shift force based on the hierarchical LQR algorithm and PI algorithm is 210N and 311N, respectively. Compared with the maximum shift force

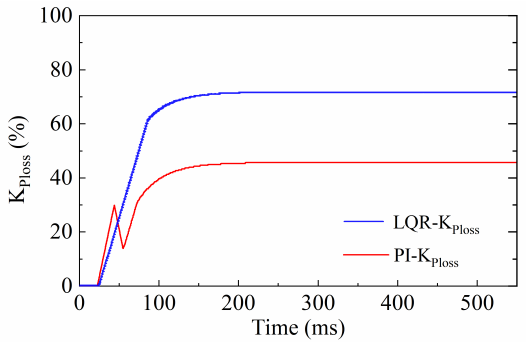

FIGURE 24. K_{ploss} curve of output shaft in engagement process.

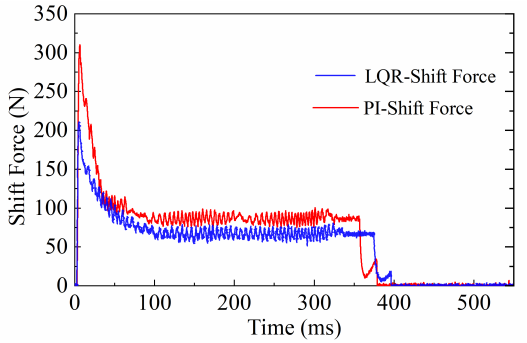

FIGURE 25. Gear-shifting force curve in engagement process.

TABLE 2. Comparison of gear shifting performance indicators based on different algorithms during upshift process.

	Time [ms]	Maximum output shaft torque gradient [Nm/s]	Maximum Kploss [%]	Maximum gear-shifting force [N]
LQR	397	-2331	71.67	210
PI	378	-2884	45.67	311
Improved index	5.03%	-19.17%	56.93%	-32.48%

based on PI algorithm, the maximum shift force based on the hierarchical LQR algorithm is reduced by 32.48%. In the whole upshift process, the gearshift force based on PI algorithm is greater than that based on HLQR algorithm.

Table 2 lists the gearshift performance indicators based on different algorithms in the upshift process, from which the following conclusions can be drawn as follows:

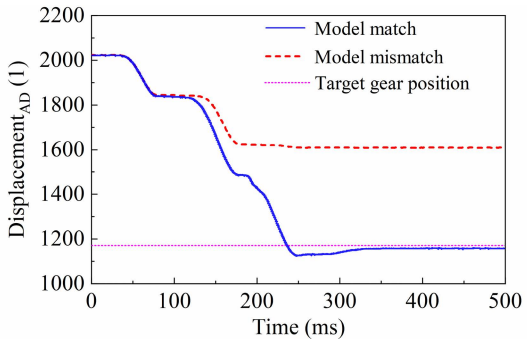

FIGURE 26. Shift actuator displacement.

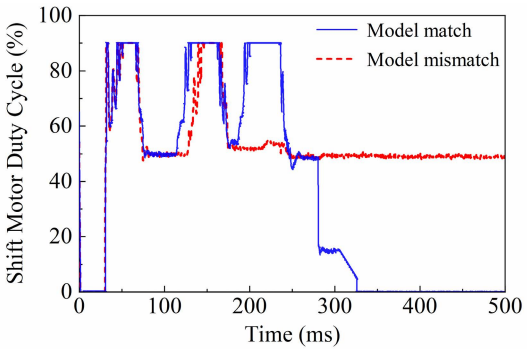

FIGURE 27. Shift motor duty cycle.

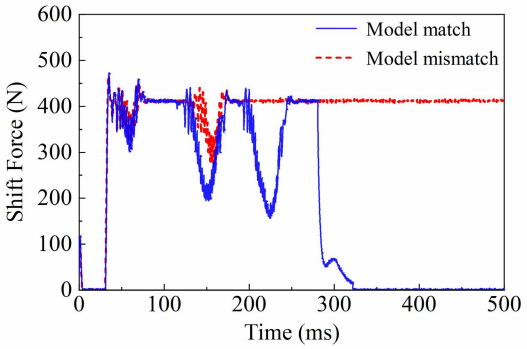

FIGURE 28. Shift forces.

C. MODEL MISMATCH ANALYSIS

The method proposed in this paper solves the problem of shift performance degradation caused by the change in output shaft speed due to external load on the system. The accuracy of the model is a prerequisite for the proposed method to exert its control effect. We designed experiments to verify the effect of model mismatch on shifting performance. During the experiment we set different model parameters to estimate the external load on the system. In the case of model mismatch, there is a relatively large deviation between the estimated result of external load and the actual value, and the method proposed in this paper does not play its ideal control effect, which makes the shift actuator stall in the downshift process, as shown in Fig.26, and the shift actuator

does not reach the target gear position, which eventually leads to shift failure. As shown in Fig.27 and Fig.28, even though there is a continuous shift force output from the shift actuator in the case of model mismatch, the shift actuator still appears to be stuck, which is caused by the insufficient torque compensation of the TM motor due to the inaccurate external load estimation.

VI. CONCLUSION

This paper provides a novel powertrain system design to suit the vehicle requirements of the 2022 Beijing Winter Olympics' particular application scenario. A hierarchical LQR algorithm is presented to handle the problem of shift quality decrease caused by the speed transformation rate of the output shaft, meanwhile improving the adaptability of the system to disturbance conditions. Simulation and bench testing are used to validate the proposed hierarchical LQR algorithm, which was then compared to existing methods. The following are the bench test results:

1) The gearshift time based on hierarchical LQR algorithm is longer than that based on PI algorithm, but the difference is not significant. The average gearshift force based on hierarchical LQR algorithm is smaller than that based on PI algorithm.
2) The maximum output shaft torque change rate based on hierarchical LQR algorithm is 19.17% lower than that based on PI algorithm. This is because the impact based on PI algorithm is a two-way impact, the shift comfort is worse than that based on hierarchical LQR algorithm;
3) The maximum output shaft power loss rate based on hierarchical LQR algorithm is 56.93% higher than that based on PI algorithm, and the dynamics performance in the shift process is slightly worse than that based on the PI algorithm, but the additional load in the shift process is reduced;
4) The maximum shift force based on hierarchical LQR algorithm is 32.48% lower than that based on PI algorithm, which can reduce the wear of actuator and synchronizer to a certain extent.

It should be pointed out that this paper solves the problem of poor shift quality due to rapid change of output shaft speed, which is caused by external disturbances-vehicle load. Accurate observation of external disturbances is an indispensable part of the method proposed in this paper. Once the observed disturbance exists deviation, the control results will exist deviation.

DECLARATION OF COMPETING INTEREST

The authors declare that they have no known competing financial interests or personal relationships that could have appeared to influence the work reported in this paper.

REFERENCES

[1] J. Wu, J. Liang, J. Ruan, N. Zhang, and P. D. Walker, "Efficiency comparison of electric vehicles powertrains with dual motor and single motor input," *Mechanism Mach. Theory*, vol. 128, pp. 569–585, Oct. 2018.

[2] L. Zhang, L. Yang, X. Guo, and X. Yuan, "Stage-by-phase multivariable combination control for centralized and distributed drive modes switching of electric vehicles," *Mechanism Mach. Theory*, vol. 147, May 2020, Art. no. 103752.

[3] M. Zeraoulia, M. E. H. Benbouzid, and D. Diallo, "Electric motor drive selection issues for HEV propulsion systems: A comparative study," *IEEE Trans. Veh. Technol.*, vol. 55, no. 6, pp. 1756–1764, Nov. 2006.

[4] L. Li, X. Li, X. Wang, J. Song, K. He, and C. Li, "Analysis of downshift's improvement to energy efficiency of an electric vehicle during regenerative braking," *Appl. Energy*, vol. 176, pp. 125–137, Aug. 2016.

[5] Q. Yu, R. Xiong, C. Lin, W. Shen, and J. Deng, "Lithium-ion battery parameters and state-of-charge joint estimation based on H-infinity and unscented Kalman filters," *IEEE Trans. Veh. Technol.*, vol. 66, no. 10, pp. 8693–8701, Oct. 2017.

[6] Z. Zhou and M. Huang, "Regenerative braking algorithm for the electric vehicle with a seamless two-speed transmission," *Proc. Inst. Mech. Eng., D, J. Automobile Eng.*, vol. 233, no. 4, pp. 905–916, 2018.

[7] C. Zhang, S. Zhang, G. Han, and H. Liu, "Power management comparison for a dual-motor-propulsion system used in a battery electric bus," *IEEE Trans. Ind. Electron.*, vol. 64, no. 5, pp. 3873–3882, May 2017.

[8] M. Zhao, J. Shi, and C. Lin, "Optimization of integrated energy management for a dual-motor coaxial coupling propulsion electric city bus," *Appl. Energy*, vol. 243, pp. 21–34, Jun. 2019.

[9] X. Xu, J. Liang, Q. Hao, P. Dong, S. Wang, W. Guo, Y. Liu, Z. Lu, J. Geng, and B. Yan, "A novel electric dual motor transmission for heavy commercial vehicles," *Automot. Innov.*, vol. 4, no. 1, pp. 34–43, Feb. 2021.

[10] M. Hu, J. Zeng, S. Xu, C. Fu, and D. Qin, "Efficiency study of a dual-motor coupling EV powertrain," *IEEE Trans. Veh. Technol.*, vol. 64, no. 6, pp. 2252–2260, Jun. 2015.

[11] S. Zhang, R. Xiong, and C. Zhang, "Pontryagin's minimum principle-based power management of a dual-motor-driven electric bus," *Appl. Energy*, vol. 159, pp. 370–380, Dec. 2015.

[12] E. Wang and F. Meng, "Down shift control with power of planetary-type automatic transmission for a heavy-duty vehicle," *Mech. Syst. Signal Process.*, vol. 159, Oct. 2021, Art. no. 107828.

[13] J. Hong, B. Gao, H. Yue, and H. Chen, "Dry clutch control of two-speed electric vehicles by using an optimal control scheme with persistent time-varying disturbance rejection," *IEEE Trans. Transp. Electrific.*, vol. 7, no. 3, pp. 2034–2046, Sep. 2021.

[14] J. Wu and N. Zhang, "Driving mode shift control for planetary gear based dual motor powertrain in electric vehicles," *Mechanism Mach. Theory*, vol. 158, Apr. 2021, Art. no. 104217.

[15] Y. Tian, N. Zhang, S. Zhou, and P. D. Walker, "Model and gear shifting control of a novel two-speed transmission for battery electric vehicles," *Mechanism Mach. Theory*, vol. 152, Oct. 2020, Art. no. 103902.

[16] S. H. Shahalami and D. Farsi, "Analysis of load frequency control in a restructured multi-area power system with the Kalman filter and the LQR controller," *AEU-Int. J. Electron. Commun.*, vol. 86, pp. 25–46, Mar. 2018.

[17] K. D. Mishra, G. Cardwell, and K. Srinivasan, "Automated calibration of gearshift controllers using iterative learning control for hybrid systems," *Control Eng. Pract.*, vol. 111, Jun. 2021, Art. no. 104786.

[18] K. Zhao, Z. Li, Y. Chen, and Y. Liu, "Multi-objective optimization of gearshift trajectory planning for multi-speed electric vehicles," *Eng. Optim.*, to be published.

[19] C. T. Nguyen, P. D. Walker, and N. Zhang, "Optimization and coordinated control of gear shift and mode transition for a dual-motor electric vehicle," *Mech. Syst. Signal Process.*, vol. 158, Sep. 2021, Art. no. 107731.

[20] W. Li, C. Kang, and X. Zhu, "Coordinated speed and position control of integrated motor-transmission system," *Trans. Inst. Meas. Control*, vol. 43, no. 13, pp. 3013–3023, Sep. 2021.

[21] Y. Tian, H. Yang, W. Mo, S. Zhou, N. Zhang, and P. D. Walker, "Optimal coordinating gearshift control of a two-speed transmission for battery electric vehicles," *Mech. Syst. Signal Process.*, vol. 136, Feb. 2020, Art. no. 106521.

[22] H. Choi, J. Hwang, and S. Choi, "Dynamic driveline torque estimation during whole gear shift for an automatic transmission," *Mechanism Mach. Theory*, vol. 130, pp. 363–381, Dec. 2018.

[23] J. Wu and N. Zhang, "Driving mode shift control for planetary gear based dual motor powertrain in electric vehicles," *Mechanism Mach. Theory*, vol. 158, Apr. 2021, Art. no. 104217.

[24] M. Roozegar and J. Angeles, "A two-phase control algorithm for gear-shifting in a novel multi-speed transmission for electric vehicles," *Mech. Syst. Signal Process.*, vol. 104, pp. 145–154, May 2018.

[25] B. Li, W. Ge, X. Yu, S. Shao, and H. Liu, "Innovative design and gearshift control for direct-drive electromagnetic gearshift system equipped with servo synchronizer," *Proc. Inst. Mech. Eng., D, J. Automobile Eng.*, vol. 233, no. 5, pp. 1115–1124, Apr. 2019.
[26] S. Kim and S. B. Choi, "Cooperative control of drive motor and clutch for gear shift of hybrid electric vehicles with dual-clutch transmission," *IEEE/ASME Trans. Mechatronics*, vol. 25, no. 3, pp. 1578–1588, Jun. 2020.
[27] S. Lin and B. Li, "Shift force optimization and trajectory tracking control for a novel gearshift system equipped with electromagnetic linear actuators," *IEEE/ASME Trans. Mechatronics*, vol. 24, no. 4, pp. 1640–1650, Aug. 2019.

CHENG LIN received the Ph.D. degree from the School of Mechanical Engineering, Beijing Institute of Technology, China, in 2002. He is currently a Professor with the School of Mechanical Engineering, Beijing Institute of Technology. His research interests include battery heating methods, thermal management systems, and electrified powertrain systems in electric vehicles.

JIANG YI received the B.S. degree from the School of Automotive Engineering, Beijing Forestry University, China, in 2014. He is currently pursuing the Ph.D. degree with the School of Mechanical Engineering, Beijing Institute of Technology, China. His current research interests include transmission control unit design and optimal control strategies.

XIAO YU received the M.S. degree in vehicle engineering from the Shandong University of Technology, China, in 2020. He is currently pursuing the Ph.D. degree with the School of Mechanical Engineering, Beijing Institute of Technology, China. His current research interests include electrified powertrain systems, energy management strategies, and collaborative control strategy for multi-motor systems.

HUIMIN LIU received the B.S. degree from the College of Engineering, China Agricultural University, China, in 2021. She is currently pursuing the M.S. degree with the School of Mechanical Engineering, Beijing Institute of Technology, China. Her current research interests include the parameter optimization of electrified powertrain systems and energy management strategies for multi-motor systems.